Two-Dimensional Photonic Crystal Confined Vertical-Cavity Surface-Emitting Lasers

Noriyuki Yokouchi, *Member, IEEE*, Aaron J. Danner, *Student Member, IEEE*, and Kent D. Choquette, *Fellow, IEEE*

***Abstract*—The two-dimensional photonic crystal (2-D PhC) structure has been investigated as a method for lateral mode control of vertical-cavity surface-emitting lasers (VCSELs). The 2-D PhC structures were designed using an equivalent index model developed for photonic crystal fibers combined with a plane wave expansion method. The etching depth dependence of the PhC structure was incorporated for the first time to design practical devices. 2-D PhC-confined VCSELs are demonstrated to operate in single PhC-confined mode using either a single- or seven-point defect.**

***Index Terms*—Surface-emitting lasers, photonic crystals, lateral mode.**

I. Introduction

LATERAL mode control of vertical-cavity surface-emitting lasers (VCSELs) is necessary not only for single-mode fiber applications but also for multimode systems. In oxide-confined VCSELs, an oxidized AlAs layer inserted into the top and/or bottom distributive Bragg reflector (DBR) produces a current and optical confinement structure. The device has a stable lateral mode due to the index confinement realized by the oxidized AlAs having a refractive index of about 1.6 [1]. But there are problems with the lateral mode characteristic of VCSELs. The spectral linewidth of oxide confined VCSELs tends to be broader compared to the linewidth of ion-implanted VCSELs. The material dispersion of silica fibers which are commonly used in optical communication systems is about 70 ps/nm/km at a wavelength of 850 nm. The typical spectral linewidth of a multimode VCSEL, which strongly depends on the size of the oxide aperture, is 1 nm or larger at higher bias current. If an optical pulse with a spectral linewidth of 1 nm transmits over 300 m, the pulse broadening is about 20 ps at the destination. The pulsewidth of a bit under nonreturn-to-zero format is 1 ns and 100 ps for 1- and 10-Gb/s operation, respectively. Since there are other contributions to the pulse broadening, the effect of the material dispersion of 20 ps is significant in 10-Gb/s transmissions, even if modal dispersion is eliminated in a high-bandwidth multimode fiber [2]. Wide-beam divergence, a common feature of oxide-confined VCSELs, is also attributed to the strong index confinement. Higher order modes having wider beam divergence are easily activated by the spatial and spectral hole burnings with nonuniform carrier injection. The wide beam shape could be a serious problem, particularly for coupling without any optics between a VCSEL and an optical fiber. Thus, a single transverse-mode VCSEL would be advantageous for multimode fiber communication systems.

For many single-mode applications, achieving sufficiently high power is critical. A single-mode VCSEL can be realized by reducing the optical aperture which satisfies the cutoff condition for any higher order modes. But the required aperture size at 850-nm wavelength is less than 3-μm diameter. It is difficult to manufacture such a small VCSEL and the electric resistance would be very high, typically more than 150 Ω, due to the tiny current injection area. Such a high electrical resistance is not acceptable for high-speed modulation. Moreover, high-power operation will not be achievable with a small emission aperture. Therefore, a variety of lateral mode control schemes have been proposed to obtain single-mode operation with enlarged emission area. Almost all lateral mode control structures reported so far [3]–[10] are based on mode selective loss/gain principles. One issue for all these structures is the additional loss for the preferred lowest order Gaussian mode.

Recently, an "endlessly" single-mode characteristic was demonstrated in a photonic crystal fiber (PCF) [11], where a single point defect acting as a waveguiding core can be enlarged by the strong wavelength dependence of an equivalent index of a two-dimensional photonic crystal (2-D PhC). Although this concept has already been applied to VCSELs [12]–[14], a robust design strategy applicable to VCSELs has not been established. The structure of a 2-D PhC confined VCSEL would be different from that of the PCF, specifically since the hole depth of the PhC structures will likely be finite to prevent degradation of the active material. An optical cavity structure with an active layer will also modify the design scheme.

In this paper, we investigate the photonic crystal structure theoretically and experimentally apply our designs to achieve single-mode VCSELs. The design concept is completely different from 2-D PhC band edge [15] or defect surface-emitting laser where lasing operation occurs laterally and the output beam is extracted vertically by diffraction. We first present the band diagram required for the device design of a semiconductor 2-D PhC structure. Next, the defect mode of an infinite-length structure (in analogy with the PCF) is obtained by neglecting the optical cavity effect. Finally, the 2-D PhC confined VCSEL structure incorporating the effect of finite hole depth and an optical cavity is evaluated and verified experimentally. Single-

Manuscript received February 26, 2003; revised July 3, 2003. This work was supported in part by a National Science Foundation Graduate Research Fellowship, and by DARPA under Award 317271-7830.

N. Yokouchi is with the Micro and Nanotechnology Laboratory, University of Illinois at Urbana-Champaign, Urbana, IL 61801 USA. He is also with The Furukawa Electric Co., Ltd., 2-4-3, Okano, Nishi-ku, Yokohama 220-0073, Japan (e-mail: nyoko@yokoken.furukawa.co.jp).

A. J. Danner and K. D. Choquette are with the Micro and Nanotechnology Laboratory, University of Illinois at Urbana-Champaign, Urbana, IL 61801 USA.

Digital Object Identifier 10.1109/JSTQE.2003.819521

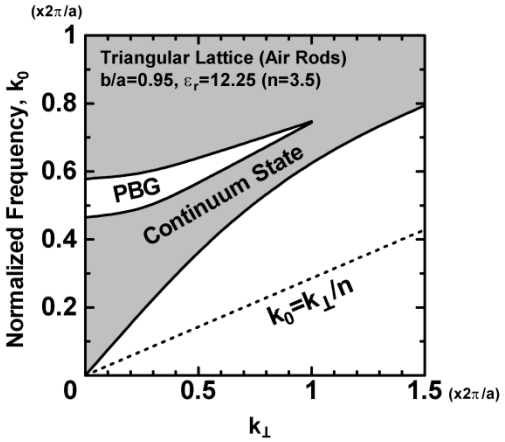

Fig. 1. Calculated photonic band diagram of a 2-D PhC structure for out-of-plane propagation.

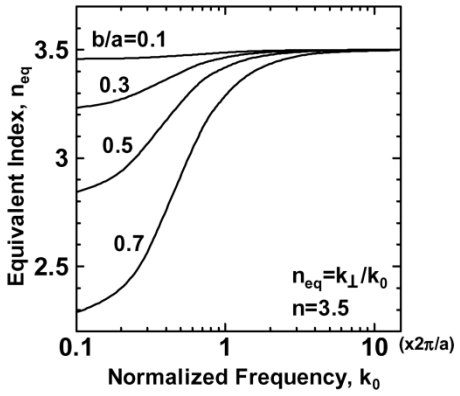

Fig. 2. Equivalent index calculated for different b/a-parameter.

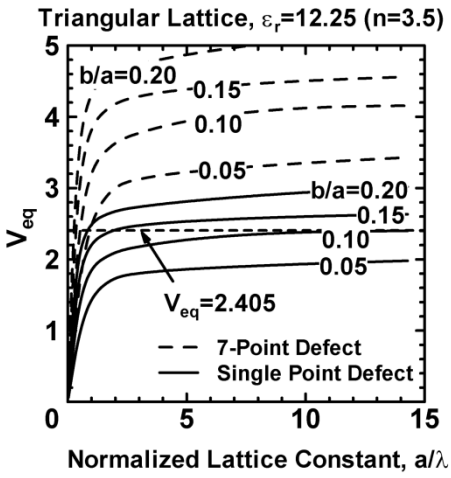

Fig. 3. Calculated $V_{\rm eq}$-parameter for single point (solid lines) and 7-point (dashed lines) defect structures with different b/a-parameter.

transverse-mode operation in a PhC confined mode in VCSELs fabricated with single- and seven-point defects are shown and discussed.

II. Band Structure Analysis

We start with the band diagram analysis of 2-D PhCs. In contrast to conventional 2-D PhC optical devices, where light propagates in the plane of the periodic structure, the band structure of the out-of-plane propagation mode [16], [17] is important for VCSEL devices where the direction of the propagation is parallel to the air rods with infinite length, in this first analysis, forming the PhC structure. We chose the plane-wave expansion (PWE) method [18], [19] to calculate the band diagram. The calculation model assumes periodic air holes with a lattice constant of a and hole diameter of b with a uniform material index of n. Although both triangular and square lattice configurations could be considered, only the former structure will be investigated in the following discussion. A typical band diagram for the out-of-plane propagation mode is shown in Fig. 1. In this calculation, b/a was chosen to be 0.95 since this structure is commonly used in optical devices relying on the photonic bandgap (PBG) effect [16]. While the photonic bandgap, denoted PBG in the figure, is open at $k_\perp = 0$, the width of the gap decreases with increasing $k_\perp$, and the gap vanishes at around $k_\perp = 1$. Even though $k_\perp$ strongly depends on the lattice constant, the typical $k_\perp$ is more than 3 assuming a VCSEL cavity having an effective refractive index of 3.5, an operating wavelength λ, and a lattice constan a, both on the order of 1 μm. Therefore, a PBG effect is not applicable for optical confinement in VCSELs.

III. Equivalent Index Model of PhC Confined Cylindrical Waveguide

The waveguiding mechanism of the PCF is refractive index reduction caused by the periodic hole array. It is known as the *effective index model* [20], but we use the term *equivalent index model* in this paper since the effective index is used as the corresponding refractive index of a VCSEL cavity as discussed in a later section. We can apply the equivalent index model to the semiconductor PhC structure. In the model, the equivalent index, which is given as $n_{\rm eq} = k_0/k_\perp$, is deduced from the lowest energy level available in the perfect PhC structure without any defects. Fig. 2 shows the calculated equivalent indexes of 2-D PhC structures with the relative hole diameter b/a as a parameter and where the material index n is assumed to be 3.5. As shown in Fig. 2, the equivalent index has a strong dependence on k_0, and thus on wavelength. This is the fundamental approach in optimizing the PhC structure to obtain a single-mode feature with large emission area. The normalized frequency, or V-parameter [21], provides information concerning the number of confined modes in a step index cylindrical waveguide. It is well known from fiber optics that the waveguide will be single mode if $V < 2.405$. The V-parameter can be modified to evaluate the single-point defect structure by using $n_{\rm eq}$ [22]

$$V_{\rm eq} = \frac{2\pi a}{\lambda}\sqrt{n^2 - n_{\rm eq}^2}. \tag{1}$$

Calculated results of $V_{\rm eq}$ with different b/a-parameters are shown in Fig. 3 where a material index n of 3.5 was used.

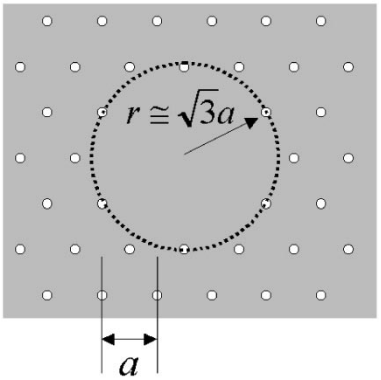

Fig. 4. The seven-point defect structure is schematically shown. Effective radius of the defect site is assumed to be $\sqrt{3}a$.

By using b/a below 0.10, the single-point defect site acts as a single-mode waveguide at the region of normalized lattice constant a/λ below 15. For the seven-point defect structure shown in Fig. 4, $V_{\rm eq}$ can be approximated to be

$$V_{\rm eq} = \frac{2\pi\sqrt{3}a}{\lambda}\sqrt{n^2 - n_{\rm eq}^2}. \tag{2}$$

The calculated $V_{\rm eq}$-parameter is also shown in Fig. 3. It is apparent from (2) that $V_{\rm eq}$ for a seven-point defect structure is $\sqrt{3}$ times larger than that of the single-point defect. From the analysis described so far, the single-point defect structure is the best one for realizing a single-mode waveguide if infinite hole depth is assumed.

We also confirm single-mode characteristic by reconstructing the optical mode field distribution obtained from the PWE method. For this calculation, the concept of a supercell structure is introduced to incorporate the defect structure. In our calculation model, the central photonic atom (air hole) within a 4×4 supercell is removed. If b/a is set to be 0.10, $V_{\rm eq}$ is estimated to be 2.2 so that the structure should be a single-mode waveguide. The optical field of the lowest energy level, which is doubly degenerate, is shown in Fig. 5. Optical fields of the first and second higher levels are also shown in the figure. These latter two levels are radiation modes, as are all higher order modes, exhibiting optical fields penetrating into the entire 2-D PhC cladding region. On the other hand, a b/a of 0.85 corresponding to $V_{\rm eq}$ of 16 supports several confined modes as shown in Fig. 6. As shown in these figures, the lowest vertical propagation mode is a Gaussian-like mode. This is different from a single-point defect laser with a lateral cavity realized by the photonic bandgap effect, where a monopole mode has a minimum of the electric field at the center of the defect [23].

IV. Etching Depth Dependence of Effective Index

In the theoretical model previously discussed, the air holes are assumed to have infinite depth. This is clearly not practical and is undesirable since nonradiative recombination could occur at the exposed sidewalls of the VCSEL active region if the holes actually extended into a bottom DBR. To optimize a 2-D PhC pattern for a realistic structure, the etching depth dependence of an effective index VCSEL cavity is discussed

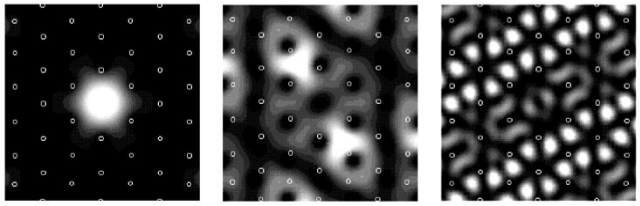

Fig. 5. Optical field distributions of the three lowest order modes are calculated for the structure with b/a of 0.1. This structure with $V_{\rm eq}$ of 2.2 has only one confined mode, which is doubly degenerated.

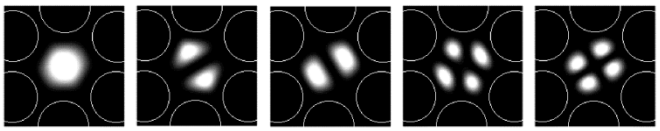

Fig. 6. Optical field distributions of the five lowest order modes of the structure with b/a of 0.85. Since $V_{\rm eq}$ of the structure calculated to be 16 there are several confined modes.

in this section. The effective index of a VCSEL cavity [22], which is different from the material index, is evaluated from the resonant cavity wavelength. The resonant wavelength is affected by perturbations due to the oxide structure, phase mismatch introduced by layer thickness uncertainty, and variation of the cavity length [22]. The formation of a 2-D PhC pattern with finite etching depth also changes the effective index. To investigate the effective index change experimentally, we made 2-D PhC patterns with different structural parameters on the surface of a VCSEL wafer and measured their resonant wavelengths [24]. The epitaxial material consists of 25-pairs of $Al_{0.9}Ga_{0.1}As/Al_{0.2}Ga_{0.8}As$ top DBR, λ-cavity, and 35.5 pairs of bottom DBR. PhC patterns were delineated by electron-beam (EB) lithography, and fabricated by using an inductively coupled plasma reactive-ion etching (ICP-RIE) technique with $SiCl_4$ as the etching gas. Since the etching depth is affected by the hole diameter, the etching depth is evaluated using a scanning electron microscope (SEM). We use a multimode optical fiber to irradiate the PhC patterns with a halogen lamp as a broad-band light source. The reflection back from the pattern is collected through the same fiber, which is split at a 3-dB coupler so that the spectra could be evaluated. To eliminate the material thickness variation across the wafer, the reflectivity of unetched regions surrounding a given PhC pattern are also evaluated.

The resonant wavelength can be calculated by a matrix transfer method. Here, however, we can use material indexes modified by the 2-D PhC structure for the layers having periodic holes. Although the thickness of each layer in a DBR is thin compared to the operating wavelength, we assume that the equivalent index deduced by the band diagram calculation is applicable to material index of the DBR. We also assume the same amount of refractive index change Δn for both the high- and low-index layers in the DBR.

Fig. 7 shows the etching depth dependence at the resonant wavelength with different b/a-parameters where lattice constant a was chosen to be 5 μm. Three lines shown in the figure denote the theoretical estimate derived by the model mentioned

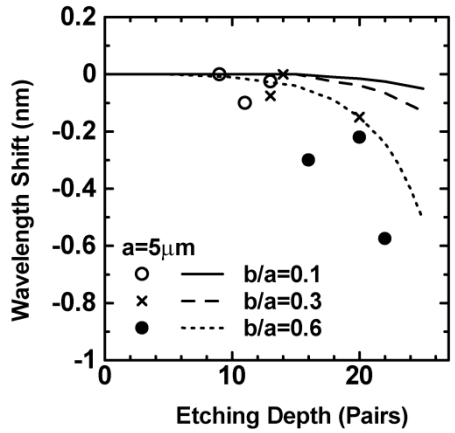

Fig. 7. Experimental and theoretical resonant wavelength shifts are plotted against etching depth. These structures have the same lattice constant of 5 μm, but different b/a-parameters.

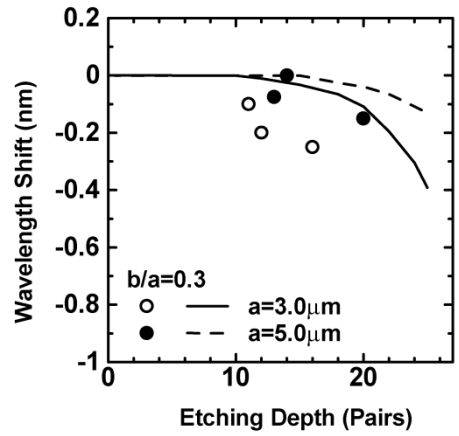

Fig. 8. Experimental and theoretical resonant wavelength shifts are plotted against etching depth. These structures have different lattice constant of 3 and 5 μm, and the same b/a of 0.3.

above. Structures with a larger hole diameter of 3.0 μm exhibit a larger blue shift. It is attributed to substantial refractive index reduction as well as the etching depth enhancement. The lattice constant dependence of the wavelength shift is compared in Fig. 8, where the two structures have the same b/a of 0.3 but different lattice constants of 3.0 and 5.0 μm, respectively. As predicted by the theoretical model, the smaller lattice constant structure produced a larger wavelength shift. In the actual samples, the etching might stop at a random depth within a DBR layer, producing a phase mismatch at the etched surface. Also, the vertical profile of the holes is different from that of the perfect holes assumed in the theoretical model. In spite of these and other limitations, the magnitude of the wavelength shift is in good agreement with our theoretical prediction.

If we translate the theoretical curves shown in Figs. 7 and 8 into the effective index change Δn_{eff} normalized by the material index reduction Δn, then all of our results have the same etching depth dependence, as shown in Fig. 9. By using the etching depth dependence factor γ, the effective index of the

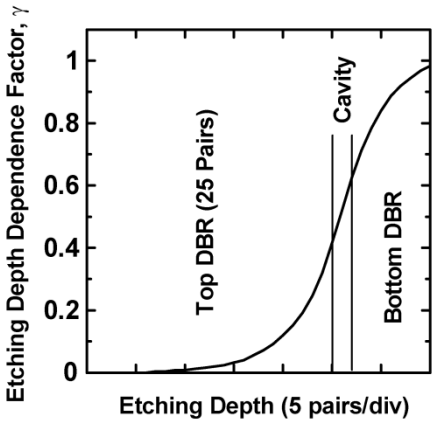

Fig. 9. Etching depth dependence factor reflecting the optical power profile along the VCSEL cavity is calculated, where 25-pair of top DBR was assumed.

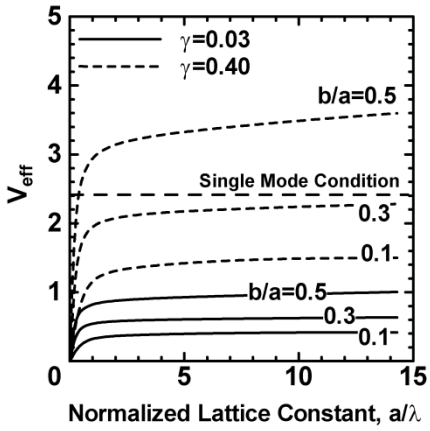

Fig. 10. V_{eff}-parameter was calculated by incorporating the etching depth dependence. γ of 0.03 and 0.4 corresponds to the etching depth of 15 and 25 pairs of top DBR, respectively.

VCSEL structure with a 2-D PhC pattern on its surface can be rewritten as

$$n'_{\text{eff}} = n_{\text{eff}} - \gamma \Delta n \tag{3}$$

where γ varies from 0 to 1 depending on the etching depth and structure. This parameter is qualitatively proportional to the optical power profile along the longitudinal VCSEL cavity. To enhance the effective index reduction using a PhC structure, the etching should be deep enough to significantly overlap the optical power distribution. The V_{eq}-parameter for the single-point defect structure can be modified to

$$V_{\text{eff}} = \frac{2\pi a}{\lambda}\sqrt{n_{\text{eff}}^2 - (n_{\text{eff}} - \gamma \Delta n)^2}. \tag{4}$$

Typical results of a V_{eff} calculation for γ of 0.03 and 0.4, which correspond to etching depths of 15 and 25 pairs, respectively, of the top DBR, are shown in Fig. 10. As is evident from the figure, V_{eff} is strongly influenced by γ. To obtain stable single-mode operation, V_{eff} should be close to 2.405 to overcome any external perturbations, such as carrier injection or thermal effects. An etching depth of 15–20 pairs, producing a γ of 0.03–0.12, is

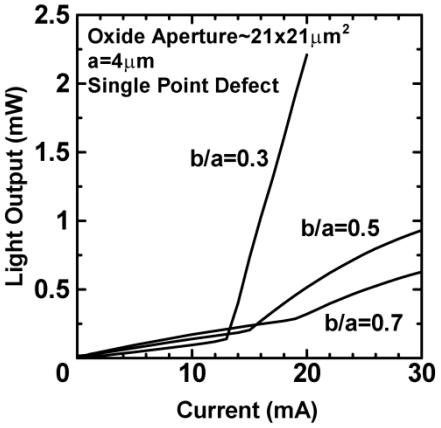

Fig. 11. Typical light output and current characteristics of fabricated PhC-confined VCSELs with a single-point defect structure.

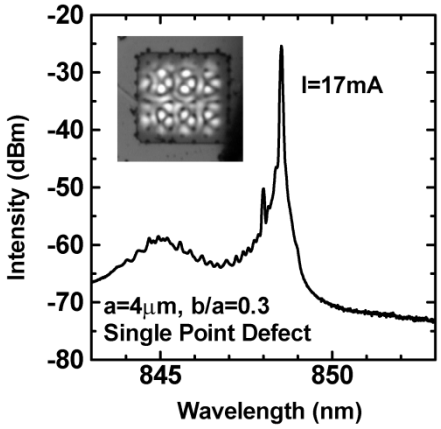

Fig. 12. Lasing spectrum and NFP of the device operating with oxide-confined modes.

reasonable for 25-pair DBR structure to avoid any risks ofdeteriorating the active region. To increase V_{eff} which has been diluted by such small γ, a relatively large b/a-parameter [12], [13] and/or a seven-point defect structure as discussed in Section III can be adopted.

V. Experimental Verification of 2-D PhC Confined VCSELs

We have fabricated PhC-confined VCSELs as follows: A VCSEL structure with 850-nm emission wavelength was grown on a p-GaAs substrate. The material contains 25-pairs of n-type top DBR and 35.5-pairs of p-type bottom DBR. Both consist of $Al_{0.9}Ga_{0.1}As/Al_{0.2}Ga_{0.8}As$ except for a 30-nm AlAs oxidation layer inserted in the bottom DBR. 2-D PhC patterns with defect structures were fabricated using EB lithography and ICP-RIE. After metallization of top and bottom contacts, square shaped mesas were formed by conventional photolithography and ICP-RIE. Finally, the AlAs single layer was selectively oxidized to define a current aperture. A SiO_2 film was used to protect the sidewalls of the PhC holes during the oxidation process. We fabricated single-point and seven-point defect devices with b/a ratios of 0.3, 0.5, and 0.7. Lattice constants of the single point and the seven-point defect structures are 4.0 and 2.0 μm, respectively, so that the sizes of the defects are almost the same. Since the etching depth of a small hole depends on its diameter, and all devices on a wafer were etched simultaneously, holes with different diameters have different depths. Etching depths determined by a SEM are 1.68 μm for the smallest hole with a 0.6-μm diameter and 2.02 μm for the largest one with a 2.8-μm diameter. These etch depths correspond to 13 and 16 pairs, respectively, of the top DBR. We used a relatively large oxide aperture size of 21 μm $\times$ 21 μm to prevent coupling of the PhC-confined mode and an oxide-confined mode. This also helps us to easily differentiate the PhC-confined mode from oxide confined modes with larger modal size. Fig. 11 shows typical light output versus current (LI) characteristics of fabricated devices with a single-point defect structure. The device with the smallest b/a of 0.3 has the lowest threshold current, but it operated in an oxide-confined mode, which was confirmed by its spectrum and near-field pattern (NFP) as shown in Fig. 12. The other two devices have high threshold currents and low efficiencies above threshold. As will be shown later, both devices operated in PhC-confined modes. Since the optical fields of these devices were confined in central defect areas, most of the injected current for each device passed through the surrounding 2-D PhC confinement region and was wasted. The effective threshold current (assuming that the current density is uniform within the oxide aperture) is estimated to be around 1 mA. This implies that the PhC-confined mode does not suffer from excess scattering loss. The lasing spectrum of the device with b/a of 0.5 is shown in Fig. 13, confirming single-mode operation. NFPs of a device with b/a of 0.7 below and above threshold are shown in Fig. 14. Below threshold, spontaneous emission is visible through all of the periodic holes due to the reduced reflectivity. In contrast, very strong emission can be seen only in the defect site above threshold. Fig. 15 shows a typical lasing spectrum and NFP of a seven-point defect device with b/a of 0.7. Among the seven-point defect devices, b/a of 0.3 results in an oxide-confined mode and the larger hole structures operate with PhC-confined modes. In all the devices that operated in the PhC-confined mode, single-mode operation is confirmed up to 30 mA which is the maximum current in this experiment.

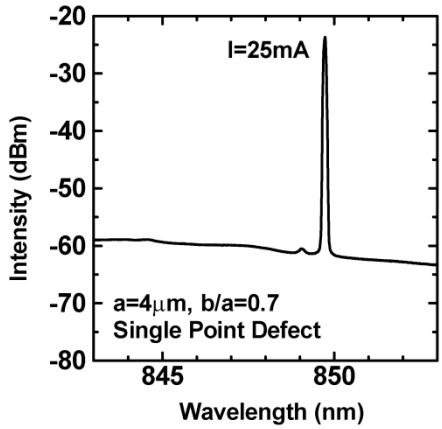

Fig. 13. Lasing spectrum of the single-point defect device with b/a of 0.7. This device operated in a single PhC-confined mode.

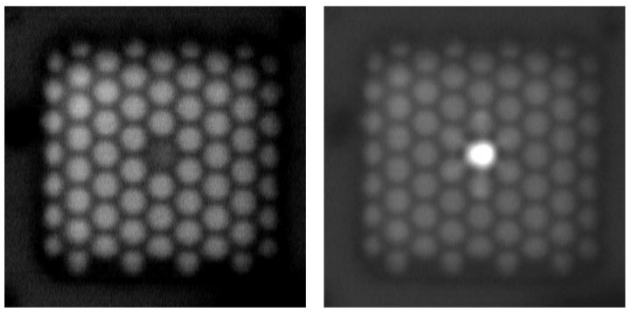

Fig. 14. NFPs below and above threshold of the device with PhC confined mode.

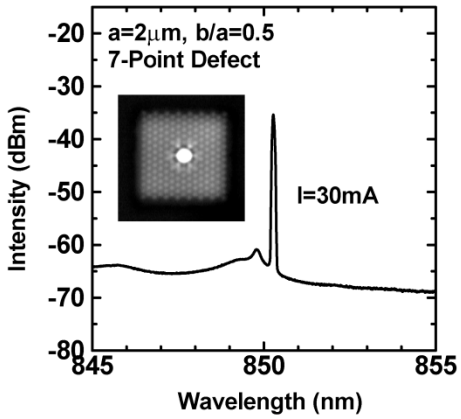

Fig. 15. Lasing spectrum and NFP of the seven-point defect device with b/a of 0.5.

Although the calculated effective refractive index change of the2-μm lattice constant structure is much larger than that of the 4-μm structure, a critical hole diameter at which the lasing mode switches from the oxide-confined to the PhC-confined modes seems to be between 0.3 and 0.5 for both structures. This result implies that the amount of the effective index step does not determine the lasing mode, but the enlarged hole diameter is mostly effective in suppressing oxide confined modes.

The weak peak appearing at a shorter wavelength than the lasing mode in Figs. 13 and 15 is reproducible in all of our devices operating in a PhC-confined mode. This wavelength splitting commonly observed in the lasing spectra is theoretically investigated as follows. The entire structure including the oxide aperture is modeled as a two-step index waveguide. By assuming the structure as a unit cell of the PWE method and for a sufficiently large unit cell to insure suppression of optical coupling between neighboring cells, optical properties (such as photon energy and optical power distribution) of guided modes can be calculated. We assume that the outer square aperture has an index step of 0.01 which is introduced by the oxidized layer. The refractive-index change obtained by the equivalent index model for the PhC is used as the inner circular index step. Theoretical results of the wavelength separations of the PhC-confined modes from the lowest oxide-confined mode are shown in Fig. 16. Judging from the etching depth, all of the experimental

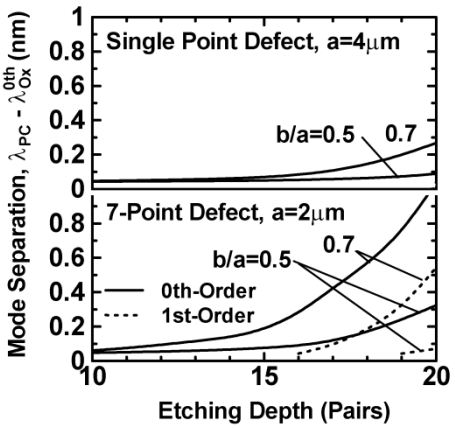

Fig. 16. Wavelength separations of PhC-confined modes from the lowest oxide confined mode are calculated.

PhC structures should be single mode. For increasing etch depth in Fig. 16, the first-order mode appears in all the structures with a seven-point defect calculated here. The wavelength separation between the fundamental and the first-order PhC-confined mode is less than 0.3 nm for the structure with b/a of 0.5 and etching depth of 20 pairs. Since the experimental separation observed in Figs. 13 and 15 is 0.5 nm and the etching depth is 14 periods, the small peak observed is thought to be one of the oxide-confined modes, neither a higher order PhC-confined mode nor the lowest oxide confined mode.

VI. Conclusion

Device design of 2-D PhC-confined VCSELs is developed by accounting for the etching depth dependence of the PhC holes. To compensate for the diluted PhC effect caused by finite etching depth, a seven-point defect structure was proposed and applied to actual VCSELs. Fabricated devices having single-point and seven-point defect structures with relatively large b/a-parameters operated in a single PhC-confined mode. Although the performance of these devices should be improved, the effective threshold current is estimated to be around 1 mA. Device performance could be significantly improved if the defect site were selectively pumped without the introduction of a large index step.

Acknowledgment

The authors acknowledge Prof. S. L. Chuang, Dr. E. W. Young, and Y. K. Kim at the University of Illinois at Urbana-Champaign for their fruitful discussions and support of this research. They also thank Dr. A. Kasukawa and N. Iwai of The Furukawa Electric Co., Ltd. for their encouragement of this study and supplying the epitaxial material.

References

[1] F. A. Kish, S. J. Caracci, N. Holonyak Jr., J. M. Dallesasse, K. C. Hsieh, M. J. Ries, S. C. Smith, and R. D. Burnham, "Planar native-oxide index-guided $Al_xGa_{1-x}As$-GaAs quantum well heterostructure lasers," *Appl. Phys. Lett.*, vol. 59, pp. 1755–1757, 1991.

[2] R. Michalzik, G. Giaretta, A. J. Ritger, and Q. L. Williams, "10 Gb/s VCSEL based data transmission over 1.6 km of new generation 850 nm multimode fiber," in *Proc. IEEE 12th Ann. Meet. LEOS'99*, San Francisco, CA, Nov. 1999. Postdeadline Paper PD1.6.
[3] H. Martinsson, J. A. Vukusic, M. Grabherr, R. Michalzik, R. Jager, K. J. Ebeling, and A. Larsson, "Transverse mode selection in large-area oxide-confined vertical-cavity surface-emitting lasers using a shallow surface relief," *IEEE Photon. Technol. Lett.*, vol. 11, pp. 1536–1538, Dec. 1999.
[4] N. Ueda, M. Tachibana, N. Iwai, T. Shinagawa, M. Ariga, Y. Sasaki, N. Yokouchi, Y. Shiina, and A. Kasukawa, "Transverse mode control and reduction of thermal resistance in 850 nm oxide confined VCSELs," *IEICE Trans. Electron.*, vol. E85-C, pp. 64–70, 2002.
[5] N. Ueki, A. Sakamoto, T. Nakamura, H. Nakayama, J. Sakurai, H. Otomo, Y. Miyamoto, M. Yoshikawa, and M. Fuse, "Single-transverse-mode 3.4 mW emission of oxide-confined 780-nm VCSEL's," *IEEE Photon. Technol. Lett.*, vol. 11, pp. 1539–1541, Dec. 1999.
[6] N. Nishiyama, M. Arai, S. Shinada, K. Suzuki, F. Koyama, and K. Iga, "Multi-oxide layer structure for single-mode operation in vertical-cavity surface-emitting lasers," *IEEE Photon. Technol. Lett.*, vol. 12, pp. 606–608, June 2000.
[7] D. G. Deppe and D. L. Huffaker, "High spatial coherence vertical-cavity surface-emitting laser using a long monolithic cavity," *Electron. Lett.*, vol. 33, pp. 211–213, 1997.
[8] E. W. Young, K. D. Choquette, S. L. Chuang, K. M. Geib, A. J. Fischer, and A. A. Allerman, "Single-transverse-mode vertical-cavity lasers under continuous and pulsed operation," *IEEE Photon. Technol. Lett.*, vol. 13, pp. 927–929, Sept. 2001.
[9] D. Zhou and L. J. Mawst, "High-power single-mode antiresonant reflecting optical waveguide-type vertical-cavity surface-emitting lasers," *J. Quant. Electron.*, vol. 38, pp. 1599–1606, 2002.
[10] S. Shinada and F. Koyama, "Single high-order transverse mode surface-emitting laser with controlled far-field pattern," *IEEE Photon. Technol. Lett.*, vol. 14, pp. 1641–1643, Dec. 2002.
[11] T. A. Birks, J. C. Knight, and P. St. J. Russell, "Endlessly single-mode photonic crystal fiber," *Opt. Lett.*, vol. 22, pp. 961–963, 1997.
[12] H. J. Unold, M. Golling, R. Michalzik, D. Supper, and K. J. Ebeling, "Photonic crystal surface-emitting lasers: Tailoring waveguide for single-mode emission," in *Proc. 27th Eur. Conf. Optical Communication*, Amsterdam, The Netherlands, 2001. Paper Th.A.1.4.
[13] D. S. Song, S. H. Kim, H. G. Park, C. K. Kim, and Y. H. Lee, "Single-fundamental-mode photonic-crystal vertical-cavity surface-emitting lasers," *Appl. Phys. Lett.*, vol. 80, pp. 3901–3903, 2002.
[14] N. Yokouchi, A. Danner, and K. D. Choquette, "Vertical cavity surface emitting lasers laterally confined by 2-dimensional photonic crystals," in *2002 Dig. LEOS Summer Topical Meetings*, Mont Tremblant, QC, Canada, July 2002. Paper TuP2.
[15] S. Noda, M. Yokoyama, M. Imada, A. Chutinan, and M. Mochizuki, "Polarization mode control of two-dimensional photonic crystal laser by unit cell structure design," *Science*, vol. 239, pp. 1123–1125, 2001.
[16] J. D. Joannopoulos, R. D. Meada, and J. N. Winn, *Photonic Crystal—Molding the Flow of Light*. Princeton, NJ: Princeton Univ. Press, 1995.
[17] A. A. Maradudin and A. R. McGurn, "Out of plane propagation of electromagnetic waves in a two-dimensional periodic dielectric medium," *J. Mod. Opt.*, vol. 41, pp. 275–284, 1994.
[18] Z. Zhang and S. Satpathy, "Electromagnetic wave propagation in periodic structure: Bloch wave solution of Maxwell's equations," *Phys. Rev. Lett.*, vol. 65, pp. 2650–2653, 1990.
[19] K. M. Ho, C. T. Chan, and C. M. Soukoulis, "Existence of a photonic gap in periodic dielectric structures," *Phys. Rev. Lett.*, vol. 65, pp. 3152–3155, 1990.
[20] J. C. Knight, T. A. Birks, and P. St. J. Russell, "Properties of photonic crystal fiber and the effective index model," *J. Opt. Soc. Amer. Ser. A*, vol. 15, pp. 748–752, 1998.
[21] G. P. Agrawal, *Fiber-Optic Communication Systems*. New York: Wiley, 1997.
[22] G. R. Hadley, "Effective index model for vertical-cavity surface-emitting lasers," *Opt. Lett.*, vol. 20, pp. 1483–1485, 1995.
[23] J. Huh, J. K. Hwang, H. Y. Ryu, and Y. H. Lee, "Nondegenerate monopole mode of single defect two-dimensional triangular photonic band-gap cavity," *J. Appl. Phys.*, vol. 92, pp. 654–659, 2002.
[24] N. Yokouchi, A. J. Danner, and K. D. Choquette, "Etching depth dependence of the effective index in two-dimensional photonic crystal patterned vertical-cavity surface-emitting laser structures," *Appl. Phys. Lett.*, vol. 82, pp. 1344–1346, 2003.

Noriyuki Yokouchi (M'94–A'95–M'01) was born in 1966. He received the B.S. degree in physical electronics engineering, and the M.S. and Ph.D. degrees in physics and information processing from Tokyo Institute of Technology, Tokyo, Japan, in 1989, 1991, and 1994, respectively. During his Ph.D. work, he demonstrated the first continuum wavelength tuning of a vertical-cavity surface-emitting laser (VCSEL) with an external mirror.

In 1994, he joined The Furukawa Electric Co., Ltd., Yokohama Research and Development Laboratories, Yokohama, Japan, where he developed several optical devices including strained-layer quantum-well lasers, waveguide photodiodes, and short- and long-wavelength VCSELs. From 2001 to February 2003, he was a Visiting Scientist at the Micro and Nanotechnology Laboratory, University of Illinois at Urbana-Champaign, where he studied photonic crystal confined VCSELs. He is an author and coauthor of more than 100 journal papers and conference articles and a coauthor of a book chapter.

Dr. Yokouchi is a member of the Institute of Electrical and Electronics Engineers/Lasers and Electro-Optics Society (IEEE/LEOS), The Japan Society of Applied Physics, and the Institute of Electronics, Information and Communication Engineers (IEICE) of Japan.

Aaron J. Danner (S'98) was born in Maryville, MO, in 1977. He received the B.S.E.E. degree from the University of Missouri-Columbia in 2000 and the M.S. degree in electrical engineering from the University of Illinois at Urbana-Champaign in 2002.

He is currently working toward the Ph.D. degree and his main research interests are photonic crystal modeling, fabrication, and single-mode VCSELs.

Mr. Danner is a student member of The Institute of Electrical and Electronics Engineers/Lasers and Electro-Optics Society (IEEE-LEOS).

Kent D. Choquette (M'97–SM'02–F'03) received the B.S. degrees in engineering physics and applied mathematics from the University of Colorado-Boulder in 1984 and the M.S. and Ph.D. degrees in materials science from the University of Wisconsin-Madison in 1985 and 1990, respectively.

In 1990, he held a postdoctoral appointment at AT&T Bell Laboratories, Murray Hill, NJ, and in 1993 he joined Sandia National Laboratories, Albuquerque, NM. He became a Professor in the Electrical and Computer Engineering Department at the University of Illinois at Urbana-Champaign in 2000. His research group is centered around the design, fabrication, and characterization of vertical-cavity surface-emitting lasers (VCSELs), photonic crystals, and other optoelectronic devices. His research interests include new microcavity light sources, nanofabrication technologies, and hybrid integration techniques. He has authored over 100 publications and three book chapters, and has presented numerous invited talks and tutorials on VCSEL's.

Prof, Choquette was an IEEE/LEOS Distinguished Lecturer from 2000 to 2002, He is an Associate Editor of the *Journal of Quantum Electronics*, a Fellow of IEEE Lasers and Electro-Optics Society (LEOS), and a member of the Optical Society of America (OSA).